Applied Catalysis B: Environmental 176–177 (2015) 454–463

Contents lists available at ScienceDirect

Applied Catalysis B: Environmental

journal homepage: www.elsevier.com/locate/apcatb

The ordered mesoporous transition metal oxides for selective catalytic reduction of NO_x at low temperature

Xiuyun Wang[a,b], Wu Wen[a], Jinxing Mi[b], Xinxiong Li[a], Ruihu Wang[a,*]

[a] State Key Laboratory of Structural Chemistry, Fujian Institute of Research on the Structure of Matter, Chinese Academy of Sciences, Fuzhou, Fujian 350002, China
[b] National Engineering Research Center of Chemical Fertilizer Catalyst, Fuzhou University, Fuzhou, Fujian 350002, China

ARTICLE INFO

Article history:
Received 7 February 2015
Received in revised form 15 April 2015
Accepted 17 April 2015
Available online 18 April 2015

Keywords:
Order mesopore
Environmental chemistry
Nanocasting method
NO_x removal
Selective catalytic reduction

ABSTRACT

The ordered mesoporous Co_3O_4, NiO and $NiCo_2O_4$ were synthesized by nanocasting method using mesoporous KIT-6 as a hard template. Their structural and textural properties were well characterized by powder X-ray diffraction, transmission electron microscopy and nitrogen physisorption. The surface areas of these catalysts are 380–426 m^2/g. Selective catalytic reduction (SCR) of NO_x with hydrogen demonstrates that $NiCo_2O_4$ possesses the highest catalytic activity at 50–400 °C, whose NO_x conversion is more than 70% at 150 °C, and N_2 selectivity is more than 90% at 100–400 °C. In addition, $NiCo_2O_4$ exhibits better stability in the presence of 100 ppm SO_2 and 10 vol% H_2O in SCR of NO_x at 250 °C. XPS analyses show that surface adsorption oxygen concentration in $NiCo_2O_4$ is higher than that in Co_3O_4 and NiO. The synergetic effect between Ni and Co is responsible for the enhancement of low-temperature SCR activity and the improvement of regeneration performance in $NiCo_2O_4$. In comparison with $NiCo_2O_4$-CP synthesized by co-precipitation method, the ordered mesoporous structure in $NiCo_2O_4$ provides larger surface area, more activated oxygen species and more reductive species, resulting in higher SCR performance at low temperature.

1. Introduction

Nitrogen oxides (NO_x) are mainly derived from stationary pollution sources and the combustion of gasoline and diesel in transportation vehicles, which are hazardous to the environment and human health [1]. A number of techniques have been developed to reduce the emission of NO_x. Among them, selective catalytic reduction (SCR) of NO_x with either hydrocarbon (HC–SCR) or ammonia/urea (NH_3–SCR) is an efficient technique to remove NO_x from diesel vehicles and stationary sources [2]. For decades, V_2O_5–WO_3 (MO_3)/TiO_2 are widely used as commercial NH_3–SCR catalysts [3]. However, many problems, such as ammonium sulfate deposition, ammonia slip, air heater fouling and high running cost, are encountered in the practical use of NH_3–SCR. In comparison with NH_3–SCR, H_2–SCR is a promising alternative in NO_x removal because of high activity toward NO_x reduction and zero emission of greenhouse gases [4], especially for industrial sites where H_2 is readily available. Therefore, it is highly desirable to replace NH_3 with non-toxic and less expensive H_2.

Pt-based and Pd-based catalysts have been revealed to possess good catalytic activity in H_2-SCR of NO_x at low temperatures [5–7]. For examples, 0.3 wt%Pt/11wt%WO_3/ZrO_2 was reported to show high NO_x conversion below 200 °C, superior N_2 selectivity of about 90%, outstanding hydrothermal stability and strong resistance against SO_2 in H_2-SCR [5a]. 100% conversion of NO and 85% N_2 selectivity were obtained in 0.1 wt%Pt/MgO–CeO_2 when 1.5 vol% H_2 was used as a reductive agent [5b,c]. NO_x conversion of 89% and N_2 selectivity of 79% at 140 °C were found in 1 wt%Pt/Ti-MCM-41 [6]. NO_x conversion of more than 80% at 140–180 °C was presented in 1 wt%Pd/TiO_2/Al_2O_3 [7a]. However, high cost of precious metals and their sensitivity to sulfur poisoning have inhibited their large-scale applications. Many efforts have been devoted to searching for the alternatives of Pt-based catalysts in H_2–SCR of NO_x.

Transition metal oxides have been widely used as catalysts in various reactions because of their low price, ready synthesis and good redox property [8]. Among them, highly ordered mesoporous materials are of particular advantages, such as regular texture, narrow pore size distribution and adjustable porous structure, which can result in promising applications in catalysis [9,10]. The nanocasting route using silica materials as hard templates is an effective method for the synthesis of ordered mesoporous transition metal oxides, the resultant oxides usually show high

* Corresponding author. Tel.: +86 591 83711028; fax: +86 591 83714946.
E-mail address: ruihu@fjirsm.ac.cn (R. Wang).

http://dx.doi.org/10.1016/j.apcatb.2015.04.038
0926-3373/

surface area and good stability under harsh reaction conditions [11]. Recently, highly ordered mesoporous Co_3O_4 was synthesized using mesoporous silica as a hard template, and displayed excellent catalytic activity for CO preferential oxidation in H_2–rich gases [12]. Compared with single metal oxides, bi- or multi-metal oxides usually show superior general properties owing to synergetic interactions of their compositions [13,14]. It is known that Ni^{2+} and Co^{2+} can form a homogeneous solid solution owing to the similarity of their unit cell structures, the replacement of Co at octahedral sites with Ni can affect the bonding strength of metal-oxygen, resulting in different adsorption energies for —OH species at catalytic sites [9,13]. The adsorbed OH can interact with NO at the interface of metal oxides, forming an intermediate NO_2 and a hydrogen atom. Therefore, a combinational use of Ni and Co oxides may result in higher catalytic activities in SCR than single metallic counterparts. However, to our knowledge, the preparation and applications of ordered mesoporous bimetal oxides in SCR of NO_x have seldom been reported. In our continuous efforts to develop low-temperature and SO_2-tolerant catalysts for NO_x removal [15], herein, we report a series of transition metal oxides with highly ordered mesopores, Co_3O_4, NiO and $NiCo_2O_4$. The catalysts show superior NO_x conversion, high N_2 selectivity, strong resistance against SO_2 and H_2O in H_2–SCR of NO_x.

2. Experimental

2.1. Catalyst preparations

Mesoporous KIT-6 was synthesized according to the literature methods [11]. Mesoporous $NiCo_2O_4$ was prepared using as-synthesized KIT-6 as a hard template. Briefly, $Ni(NO_3)_2{\cdot}6H_2O$ and $Co(NO_3)_2{\cdot}6H_2O$ (total mass:1.0 g) with the molar ratio of 1:2 were dissolved in ethanol (20 mL). After stirring at room temperature for 1 h, 0.5 g of KIT-6 was added. The suspension was stirred at room temperature for 12 h, and followed by calcination at 400 °C for 3 h, then treated with NaOH, washed and dried. The resultant sample was denoted as $NiCo_2O_4$. Mesoporous Co_3O_4 and NiO were prepared using the same procedures.

As a comparison, $NiCo_2O_4$–CP was also synthesized by co-precipitation method. A solution of $Ni(NO_3)_2{\cdot}6H_2O$ and $Co(NO_3)_2{\cdot}6H_2O$ (total mass:1.0 g) with the molar ratio of 1:2 in H_2O (20 mL) was stirred at room temperature for 1 h, NaOH (0.24 mol/L) was dropwise added until pH to 10. After the mixture was stirred at room temperature for 12 h, the precipitate was collected by centrifugation, washed with distilled water and then calcined at 400 °C for 3 h.

2.2. Catalytic activity tests

SCR activity measurement was performed in a fixed-bed stainless steel reactor (inner diameter = 8 mm). Before each test, a 0.4 g of 20–30 mesh sample was reduced by 3.5 vol% H_2/Ar at 500 °C for 2 h. After cooled to test temperature, the feed gas (342 ppm NO, 1.5 vol% H_2 and 3 vol% O_2 balanced by Ar with H_2/NO ratio at 43.9) was introduced using mass-flow controllers at a total flow rate of 600 mL/min, the corresponding GHSV is 90,000 h^{-1}. H_2/NO feed ratios at 5, 7.5, 10 and 20 were also measured under the same conditions. SO_2 poisoning experiment was performed by exposing samples to feed gas containing additional 100 ppm SO_2 at 250 °C. Resistance against H_2O was examined through introducing 10 vol% H_2O into feed gas at 250 °C. The outlet NO_x concentration was monitored by an on-line chemiluminescence NO–NO_2–NO_x analyzer (Model 42i-HL, Thermo Scientific). N_2 selectivity was analyzed using a GC 7820A. The outlet N_2O and NH_3 were analyzed using an FTIR spectrometer (Nicolet Nexus 6700) with a heated, multiple-path gas cell. NO_x conversion was calculated according to the following equation after a steady state was achieved at the given temperature for 1 h.

$$NO_x\ \text{Conversion}\ (\%) = \frac{(NO_{xinlet} - NO_{xoutlet})}{NO_{xinlet}} \times 100\%.$$

Transient response method (TRM) of mesoporous $NiCo_2O_4$ was carried out at 150 °C, a feed gas of 350 ppm NO, 3 vol% O_2 and 1.5 vol% H_2 balanced by Ar was introduced. The outlet gas concentrations were continuously monitored by mass spectrometer and UV analyzer.

2.3. Characterizations

Powder X-ray diffraction (XRD) was performed on a Rigaku-DMax2500PC diffractometer using a Cu–Kα radiation (λ = 1.5406 Å). N_2 physisorption measurement was performed on an ASAP 2020 apparatus, the sample was degassed in vacuo at 180 °C at least 6 h before each measurement. H_2 temperature-programmed reduction (H_2–TPR) was performed on AutoChem II 2920 equipped with a TCD detector, in which the sample was pretreated under air flow (30 mL/min) at 500 °C for 0.5 h, followed by purging with Ar (30 mL/min) at the same temperature for 0.5 h. After cooling to room temperature, the temperature was increased to 800 °C at 5 °C/min by a temperature-programmed controller in a gas flow of 10 vol% H_2/Ar (30 mL/min). For the repeated H_2–TPR, the sample was reduced from room temperature to 500 °C and hold at 500 °C for 0.5 h. Then, the sample was re-oxidized in 5 vol% O_2/Ar flow at 500 °C for 1 h to ensure complete oxidation of sulfides to sulfates. After cooling to room temperature, the test of the repeated H_2–TPR was performed. X-ray photoelectron spectroscopy (XPS) analysis was performed on Physical Electronics Quantum 2000, equipped with a monochromatic Al–Kα source (Kα = 1,486.6 eV) and a charge neutralizer. Transmission electron microscope (TEM) measurements were carried out on a JEM-2010 microscope operating at 200 kV in the mode of bright field.

3. Results and discussion

3.1. TEM and HR–TEM

TEM images of KIT-6 indicate that it possesses the expected cubic mesoporous structure [9], the corresponding distance between two lattice fringes is 10 nm (Fig. S1). As expected, Co_3O_4, NiO and $NiCo_2O_4$ show highly ordered mesoporous structures with particles size about 6–8 nm (Fig. 1), and the lattice fringes can be clearly observed in their HR-TEM, suggesting highly crystalline nature of mesoporous frameworks [9c]. The spacing distances between two fringes in Co_3O_4 are 0.46 and 0.24 nm, corresponding to (1 1 1) and (2 2 0) planes, respectively. The mesoporous structure of Co_3O_4 is comparable with analogues synthesized by nanocasting method [9c]. It was reported that (1 1 1) plane in Co_3O_4 mainly contains Co^{2+}, while (2 2 0) plane only consists of Co^{3+} and provides favorable sites for oxygen adsorption in catalytic reactions [11]. In NiO, the lattice spacing of 0.21 and 0.25 nm corresponds to (2 0 0) and (1 1 1) planes of cubic Fm3m crystal lattices, respectively [10b]. The distances between the adjacent fringes in $NiCo_2O_4$ are 0.47, 0.28 and 0.23 nm, which are in conformity with (1 1 1), (2 2 0) and (2 2 2) planes, respectively [10a]. Selected-area electron diffraction (SAED) patterns (insets of Fig. 1) of the catalysts indicate that NiO and $NiCo_2O_4$ are polycrystalline [10c].

3.2. Structural and textural properties

The ordered mesoporous structures of the catalysts were further demonstrated by low-angle XRD patterns. As shown in Fig. 2a,

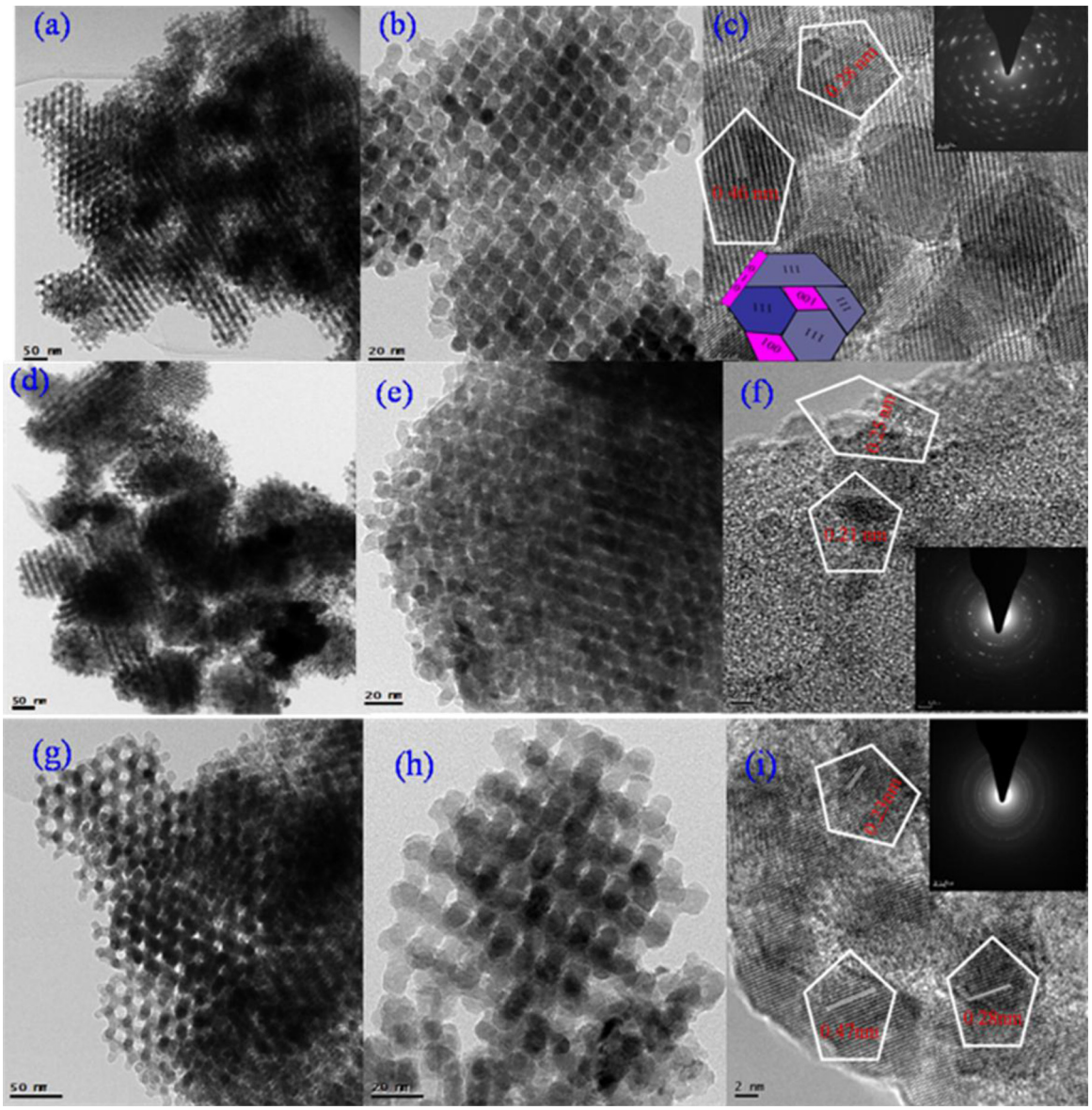

Fig. 1. TEM images of (a, b) Co_3O_4, (d, e) NiO and (g, h) $NiCo_2O_4$; HR–TEM images and SAED patterns (insets) of (c) Co_3O_4, (f) NiO and (i) $NiCo_2O_4$.

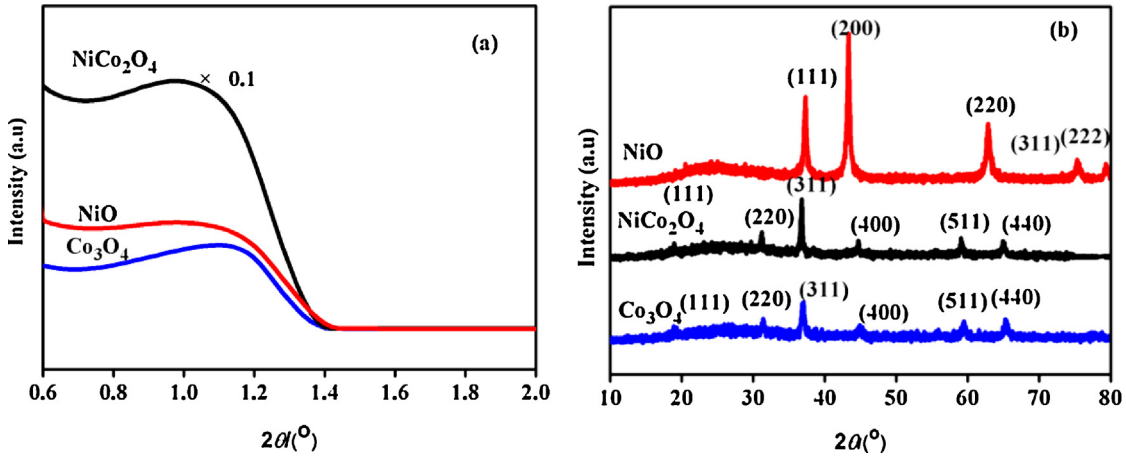

Fig. 2. Low-angle (a) and wide-angle (b) XRD patterns of Co_3O_4, NiO and $NiCo_2O_4$.

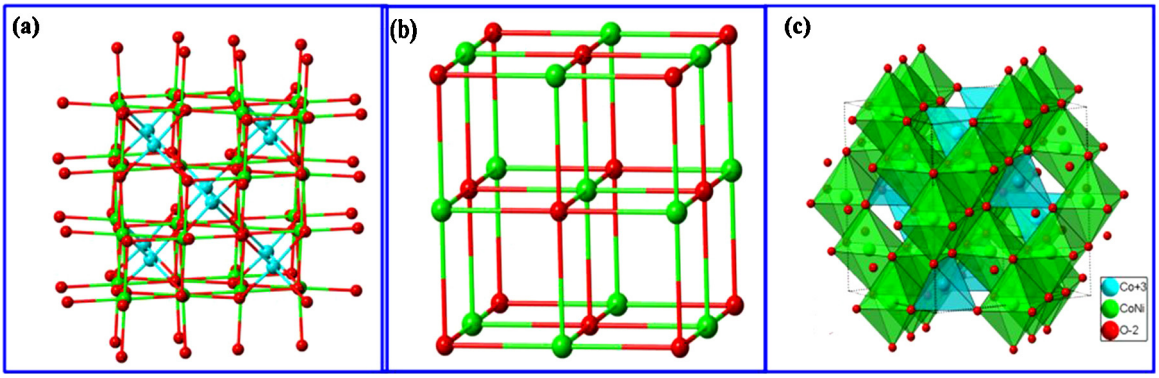

Fig. 3. The simulated structures of unit cells for (a) Co_3O_4, (b) NiO and (c) $NiCo_2O_4$.

a peak at 1.0–1.2°is observed in Co_3O_4, NiO and $NiCo_2O_4$, exhibiting the existence of well-ordered mesoporous structure, which is in good agreement with their TEM results. Notably, the peak in $NiCo_2O_4$ is much stronger than that of Co_3O_4 and NiO. The wide-angle XRD patterns of Co_3O_4, NiO and $NiCo_2O_4$ are shown in Fig. 2b. For NiO, five well-defined diffraction peaks are observed at 2θ values of 37.2, 44.5, 51.9, 76.5 and 78.9°, which can be assigned to (1 1 1), (2 0 0), (2 2 0), (3 1 1) and (2 2 2) planes of the face-centered cubic NiO structure, respectively. In Co_3O_4, the diffraction peaks at 18.9, 31.3, 36.9, 44.9, 59.4 and 65.4° could be assigned to (1 1 1), (2 2 0), (3 1 1), (4 0 0), (5 1 1) and (4 4 0) crystal planes (JCPDS No. 42-1467), respectively. The diffraction peaks of $NiCo_2O_4$ are slightly shifted to low 2θ in comparison with those of Co_3O_4, indicating a slight increment in unit cell size due to the partial substitution of Co by Ni [9c]. Interestingly, no obvious peaks of other impurities are detected in Co_3O_4, NiO and $NiCo_2O_4$, suggesting that it is appropriate to generate single phases by calcination of the catalyst precursors at 400 °C for 3 h. Pictures of the simulated structures of their unit cells are shown in Fig. 3, Co_3O_4 has a spinel structure, in which Co^{3+} and Co^{2+} are in the octahedral and tetrahedral coordination, respectively, while NiO spinel structure only contains Ni^{2+} of hexahedral coordination. For $NiCo_2O_4$ cubic spinel, Ni occupies the octahedral coordination sites, and Co is distributed over both octahedral and tetrahedral sites [9b], which affect the binding strength of metal-oxygen and surface oxygen vacancies.

N_2 physisorption was performed to study textural properties of these catalysts. As shown in Fig. 4, nitrogen adsorption–desorption isotherms in Co_3O_4, NiO and $NiCo_2O_4$ show a typical type-IV curve with hysteresis loops, suggesting the existence of mesopores [16]. For NiO and $NiCo_2O_4$, the capillary condensation occurs in the relative pressure from 0.60 to 0.80 and from 0.45 to 0.85, respectively. However, the capillary condensation in Co_3O_4 is observed in the relative high pressure ranging from 0.8 to 1.0, suggesting that porous structures in $NiCo_2O_4$ and NiO are quite open, and there are no significant delays in the capillary evaporation with respect to the capillary condensation of nitrogen when compared with that in Co_3O_4 [11]. For Co_3O_4, the pore size under 10 nm mainly results from the pores in the sidewalls, while the pore size above 10 nm may be due to partial filling of one set of pores in mesoporous KIT-6 template [17]. $NiCo_2O_4$ shows the maximum pore sizes at 2.2 and 3.7 nm, and NiO gives the maximum sizes at 3.4 and 7.4 nm. As shown in Table 1, BET surface area and pore volume of Co_3O_4, NiO and $NiCo_2O_4$ are in the range of 380–426 m^2/g and 0.23–0.37 cm^3/g, respectively, which are much higher than those of $NiCo_2O_4$–CP (27 m^2/g and 0.11 cm^3/g). The high BET surface area and large pore volume provide a possibility to obtain good SCR performance.

Table 1
Textural properties of Co_3O_4, NiO, $NiCo_2O_4$ and $NiCo_2O_4$–CP.

Sample	BET surface area (m^2/g)	Pore volume (cm^3/g)	Average pore diameter (nm)
Co_3O_4	419	0.37	4.62
$NiCo_2O_4$	426	0.36	2.92
NiO	380	0.23	3.41
$NiCo_2O_4$–CP	27	0.11	12.73

3.3. SCR activity test

It is well known that the oxidation of NO to NO_2 is an important process for NO_x reduction. NO to NO_2 conversion in Co_3O_4, NiO, $NiCo_2O_4$ and $NiCo_2O_4$–CP are shown in Fig. 5a. For all catalysts, NO-to-NO_2 conversion at low temperatures is low due to kinetic limitation, and reaches the maximum at 350 °C, then a subsequent drop of conversion is observed due to thermodynamic limitation. Obviously, NO-to-NO_2 conversion is enhanced after Co is partially substituted by Ni, which may be related to the variation in the bonding strength of metal—oxygen and surface oxygen vacancies [9c], ultimately influencing the oxidation of NO to NO_2. Interestingly, NO to NO_2 conversion in $NiCo_2O_4$ is higher than that of $NiCo_2O_4$–CP, which may be attributed that the ordered mesoporous structures provide larger surface area and more activated oxygen species. The catalytic activities of Co_3O_4, NiO, $NiCo_2O_4$ and $NiCo_2O_4$–CP in H_2–SCR of NO_x are presented in Fig. 5b. NO_x conversions of Co_3O_4 and NiO show negligible variation from 50 to 100 °C, and begin to gradually enhance after 100 °C, the maximum of 99% is reached at 250 and 200 °C, respectively. Notably, NO_x conversion of $NiCo_2O_4$ immediately increases as the temperature is elevated from 50 °C, and reaches the maximum of 99% at 200 °C. Generally, NO_x conversion at 50–200 °C follows the order: $NiCo_2O_4$ > NiO > Co_3O_4. This trend may be related to the difference of redox properties in transition metal oxides [18]. NO_x conversions at 100 °C in Co_3O_4, NiO and $NiCo_2O_4$ are 20, 27 and 38%, respectively, which are increased to 34, 52 and 75% at 150 °C, respectively. Apparently, $NiCo_2O_4$ shows higher NO_x conversion than Co_3O_4 and NiO at low temperature, which probably results from strong interactions between Ni and Co ions, leading to the abundance of the active oxygen species and the difference of the redox behavior. Notably, $NiCo_2O_4$–CP shows a lower NO_x conversion at 50–250 °C than the ordered mesoporous $NiCo_2O_4$. The superior NO_x conversion in $NiCo_2O_4$ is related to highly ordered mesoporous structures. It should be mentioned that NO_x conversion in these catalysts is more than 99% at 250–400 °C, and N_2 selectivity maintains more than 90% in 100–400 °C (Fig. S2). In mesoporous $NiCo_2O_4$, N_2O and NH_3 selectivities at 50–400 °C are less than 4% and 11%, respectively (Fig. S2b). H_2 conversion is less than 50% at 50–100 °C, and reaches more than 99% at 150–400 °C (Fig. S3). These results suggest that H_2 conversion is mainly ascribed

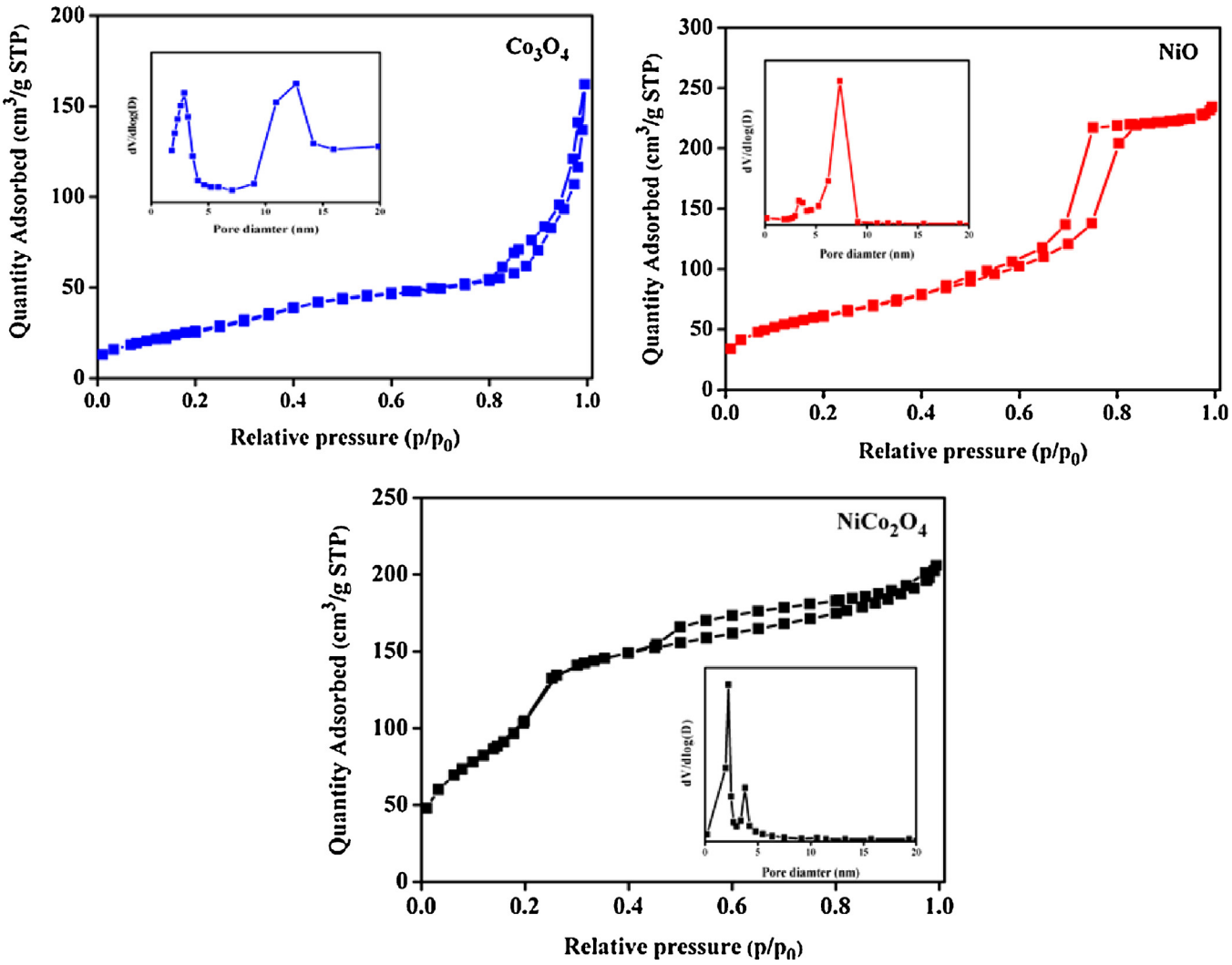

Fig. 4. N_2 physisorption isotherms and pore-size distribution curves (insert) of Co_3O_4, NiO and $NiCo_2O_4$.

to hydrogen combustion, and only a small amount of H_2 takes part in the reduction of NO_x.

H_2–SCR performance of the catalysts was reported to be associated with the ratios of H_2/NO [5b], the effects of H_2/NO feed ratios on NO_x conversion were further investigated using $NiCo_2O_4$. As shown in Fig. S4a, NO_x conversion is apparently enhanced as H_2/NO feed ratio increases. For instances, H_2/NO ratios of 5, 7.5, 10, 20 and 43.9 at 200 °C gave rise to NO_x conversions of 67, 77, 82, 84 and 99%, respectively. The promotion may be ascribed to the enhancement of NO dissociation rate owing to more surface coverage of H in gas

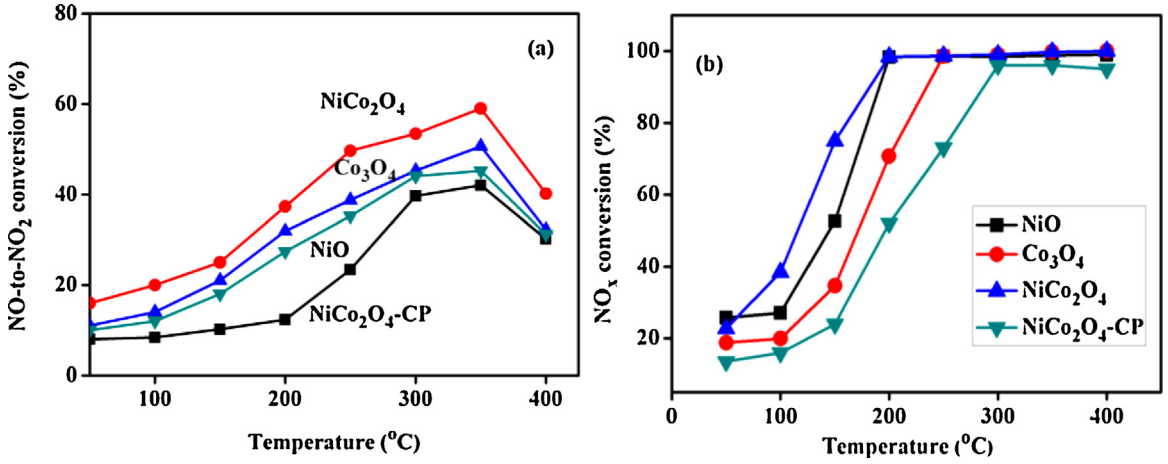

Fig. 5. (a) NO to NO_2 conversion and (b) NO_x conversion of Co_3O_4, NiO, $NiCo_2O_4$ and $NiCo_2O_4$–CP at different temperatures.

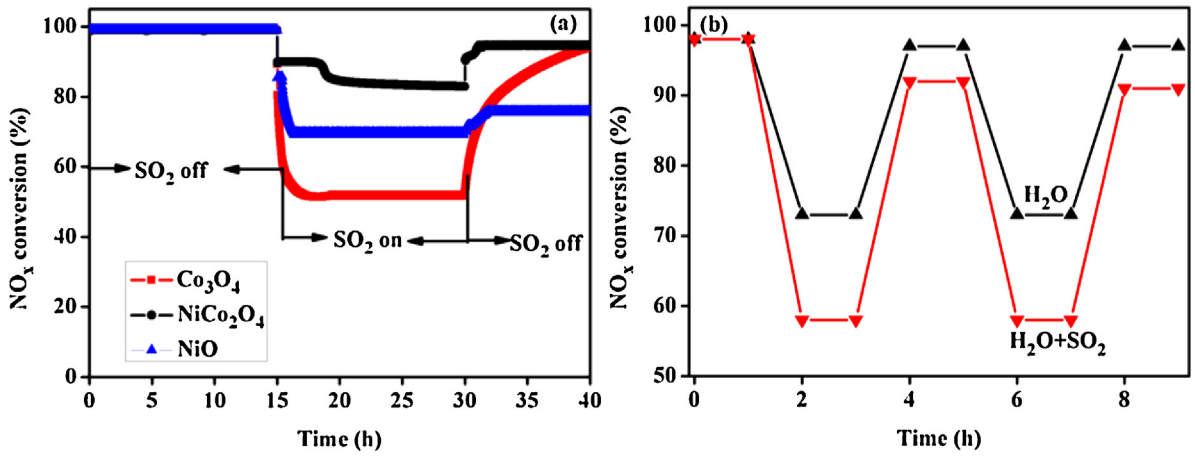

Fig. 6. (a) Stability test, SO_2 poisoning and regeneration of the catalysts at 250 °C; (b) the effect of H_2O and $H_2O + SO_2$ on NO_x conversion of $NiCo_2O_4$ at 250 °C.

phase [5d]. NO_x conversions in Co_3O_4 and NiO with H_2/NO ratio of 10 are shown in Fig. S4b. As expected, NO_x conversion follows the order: $NiCo_2O_4$ > NiO > Co_3O_4, which is consistent with that from the original ratio of H_2/NO at 43.9 (Fig. 5b).

It was reported that NH_4NO_3 can be formed at low temperature owing to simultaneous existence of NH_3 and NO_2 in exhaust gases [3d]. TRM of mesoporous $NiCo_2O_4$ was conducted at 150 °C to indirectly estimate the amount of NH_4NO_3 according to N-balance. When a feed gas of 350 ppm NO, 3 vol% O_2 and 1.5 vol% H_2 balanced by Ar was introduced into the system, the outlet NO_x ($NO + NO_2$) concentration is 87 ppm. After the system reaches a steady state, the formed N_2, N_2O and NH_3 are 121, 3 and 8 ppm, respectively (Fig. S5). The lack of 7 ppm in the total amount of N evidences the formation of 3.5 ppm NH_4NO_3 in $NiCo_2O_4$.

The simultaneous existence of SO_2 and H_2O in exhaust gases is known as one deactivation cause of SCR catalysts at low temperature due to the formation of sulfite/sulfate [14], the improvement of SO_2 and H_2O tolerance is one of challenges in SCR of NO_x. SO_2 tolerance of Co_3O_4, NiO and $NiCo_2O_4$ was examined in feed gas containing the additional 100 ppm SO_2 at 250 °C. As illustrated in Fig. 6a, NO_x conversion in Co_3O_4, NiO and $NiCo_2O_4$ at 250 °C maintains 99% in the absence of SO_2. However, the presence of 100 ppm SO_2 results in a quick decrement of NO_x conversion from 99 to 52, 69 and 83%, respectively. After the supply of SO_2 is cut off, their NO_x conversion returns to 94, 75 and 94%, respectively, suggesting Co_3O_4 and $NiCo_2O_4$ possess relatively better regeneration ability than NiO. NO_x conversion was also tested in feed gas containing 10 vol% H_2O at 250 °C. The presence of H_2O leads to a decrement of NO_x conversion from 98 to 73% in $NiCo_2O_4$ (Fig. 6b). After cutting off the supply of H_2O, NO_x conversion is restored to 98% at 250 °C. The co-existence of 10 vol% H_2O and 100 ppm SO_2 results in a decrement of NO_x conversion from 98 to 58% in $NiCo_2O_4$. However, NO_x conversion is not recovered completely after the removal of SO_2 and H_2O, which is restored only to 91%.

3.4. TEM and XRD after SCR test

In order to investigate stability of these mesoporous catalysts after SCR test, XRD and TEM analyses of the aged Co_3O_4, NiO and $NiCo_2O_4$ were carried out. As shown in Fig. 7, their TEM images show the particle sizes of the aged catalysts slightly increase, but the mesoporous structures are almost maintained after H_2–SCR. The main characteristic peaks of Ni species are observed in XRD spectrum of the aged NiO. Particle size in the aged NiO, estimated with Scherrer equation from the broadening of characteristic peak at $2\theta = 44.5$, is 25.8 nm, which is nearly twice as much as that from TEM results (ca.14 nm). Ni, $NiCo_2O_4$ and $NiCoO_2$ species are found in the aged $NiCo_2O_4$, while CoO and Co_3O_4 species co-exist in the aged Co_3O_4.

Table 2
Data of H_2–TPR profiles for Co_3O_4, NiO, $NiCo_2O_4$ and $NiCo_2O_4$–CP.

Sample	Peak position (°C)		Total H_2 consumption (mmol/g)
	T_1	T_2	$n_1 + n_2$
Co_3O_4	352	674	1.61
NiO	338	–	6.54
$NiCo_2O_4$	253	323	9.90
$NiCo_2O_4$–CP	250	354	3.94

3.5. H_2–TPR analysis

In order to clarify correlation between redox property and SCR performance, Co_3O_4, $NiCo_2O_4$, NiO and $NiCo_2O_4$–CP were characterized by H_2–TPR. As shown in Fig. 9, there are two well-defined reduction peaks in Co_3O_4, which correspond to stepwise reduction of Co_3O_4. The first peak at 352 °C is attributed to the reduction of Co_3O_4 to CoO, and the second at 674 °C is related to the reduction of CoO to Co° [10c]. It is noteworthy that only a broad reduction peak at 338 °C is found in NiO, which is attributed to the reduction of NiO to Ni. H_2–TPR profile of $NiCo_2O_4$ exhibits one weak peak at 253 °C and one strong peak at 323 °C. The former is assigned to the reduction of $NiCo_2O_4$ to $NiCoO_2$, while the latter corresponds to the co-reduction of Ni^{2+} to Ni and Co^{2+} to Co, which are overlapped to form a strong and broad peak. These results are in good agreement with XRD analyses of the aged $NiCo_2O_4$ (Fig. 8). It should be mentioned that the reduction peaks of $NiCo_2O_4$ shift to lower temperatures than those of Co_3O_4 and NiO, further indicating the presence of a strong interaction between Co and Ni in $NiCo_2O_4$, resulting in the improvement of low-temperature reducibility. It would be beneficial for H_2–SCR since the reduction of NO_x is proceeded via a Mars-van Krevelen (redox) mechanism [19]. H_2 consumptions of Co_3O_4, $NiCo_2O_4$ and NiO are listed in Table 2. The total amount of H_2 consumption in $NiCo_2O_4$ is 9.90 mmol/g, which is much higher than that of Co_3O_4 (1.61 mmol/g) and NiO (6.54 mmol/g), implying that $NiCo_2O_4$ possesses superior reduction ability at low temperature. In addition, H_2 consumption in mesoporous $NiCo_2O_4$ is much higher than that of $NiCo_2O_4$–CP (3.94 mmol/g), indicating mesoporous catalysts expose more reductive species, which are beneficial to improve SCR performance at low temperature.

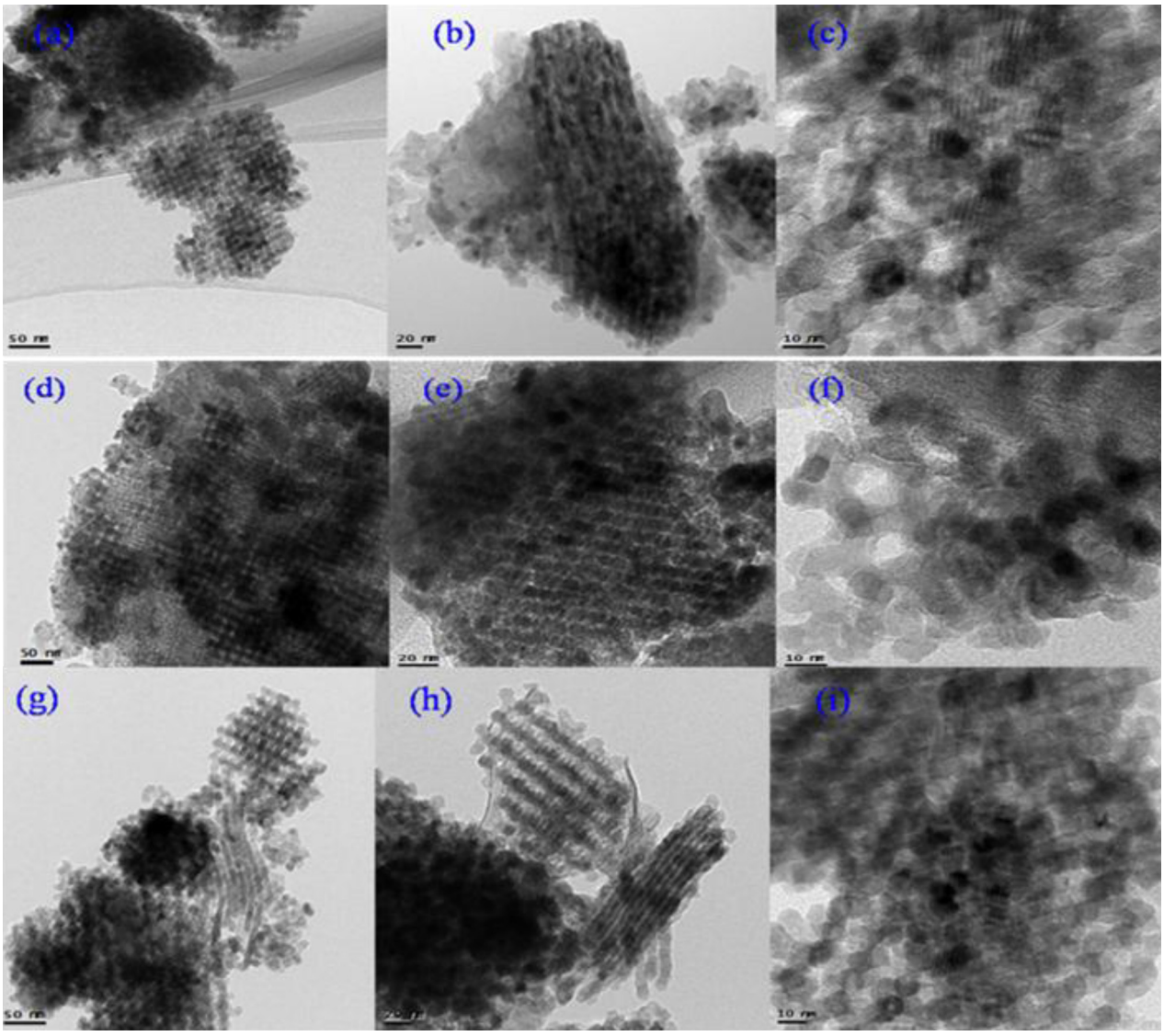

Fig. 7. TEM images of (a–c) Co_3O_4, (d–f) NiO and (g–i) $NiCo_2O_4$ after SCR test.

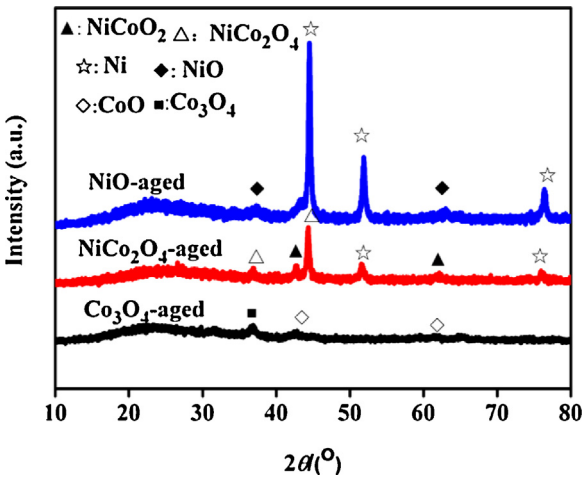

Fig. 8. XRD patterns of Co_3O_4, NiO and $NiCo_2O_4$ after SCR test.

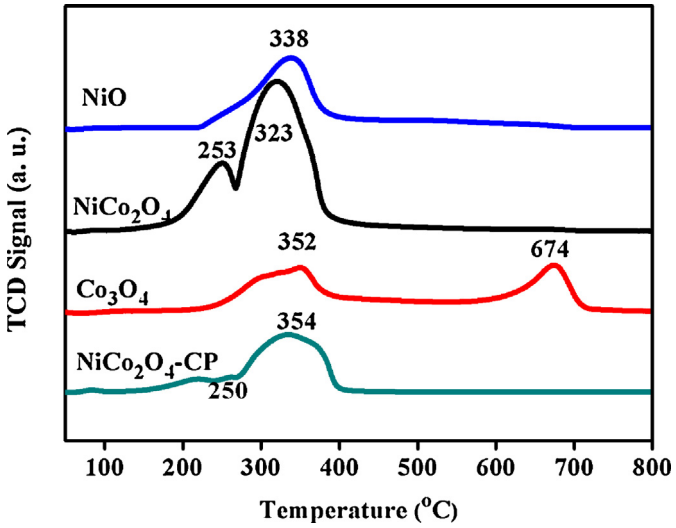

Fig. 9. H_2–TPR profiles of Co_3O_4, NiO, $NiCo_2O_4$ and $NiCo_2O_4$–CP.

Table 3
Surface valence state, S content, Co^{2+}/Co^{3+} and $O_{ads}/(O_{latt}+O_{ads})$ molar ratio.

Sample	Surface valence state	Co^{2+}/Co^{3+} molar ratio (%)	$O_{ads}/(O_{latt}+O_{ads})$ (%)	S 2p content [a] (%)
Co_3O_4	Co^{2+}, Co^{3+}	0.48	62.12	0.24 (0.11)
$NiCo_2O_4$	Ni^{2+}, Ni^{3+}, Co^{2+}, Co^{3+}	0.62	75.06	0.28 (0.11)
NiO	Ni^{2+}	–	63.76	0.30 (0.25)
$NiCo_2O_4$–CP	Ni^{2+}, Ni^{3+}, Co^{2+}, Co^{3+}	–	26.71	–

[a] The values in parentheses are from the regenerated catalysts.

3.6. XPS analysis

XPS is an effective technique to gain information of surface element compositions, metal oxidation states and the adsorbed species of a catalyst [20]. As shown in Fig. 10, XPS spectrum of Ni $2p_{3/2}$ shows that Ni^{2+} is the predominant specie in NiO, which is in good agreement with XRD and H_2–TPR results. However, the co-existence of Ni^{2+} and Ni^{3+} is observed in $NiCo_2O_4$. XPS spectra of $Co2p_{3/2}$ in Co_3O_4 and $NiCo_2O_4$ show two main peaks of binding energies at 780.2 and 784.2 eV, respectively, which are assigned to the surface Co^{3+} and Co^{2+} species, respectively [21]. The surface Co^{2+}/Co^{3+} molar ratio in $NiCo_2O_4$ is 0.62, which is higher than that of 0.48 in Co_3O_4 (Table 3).

The oxygen vacancies are known to play an important role in catalytic reactions [22], since the oxygen vacancies on catalyst surface may accelerate the adsorption and dissociation of oxygen molecules, resulting in the formation of highly active electrophilic oxygen molecules [10c]. It was reported that reducibility of metal oxides is closely associated with oxygen vacancies. The higher reduction ability in a metal oxide, the easier surface oxygen vacancies can be induced [10c]. In O1s XPS spectra of Co_3O_4, NiO and $NiCo_2O_4$ (Fig. 10), there are two peaks of binding energies,

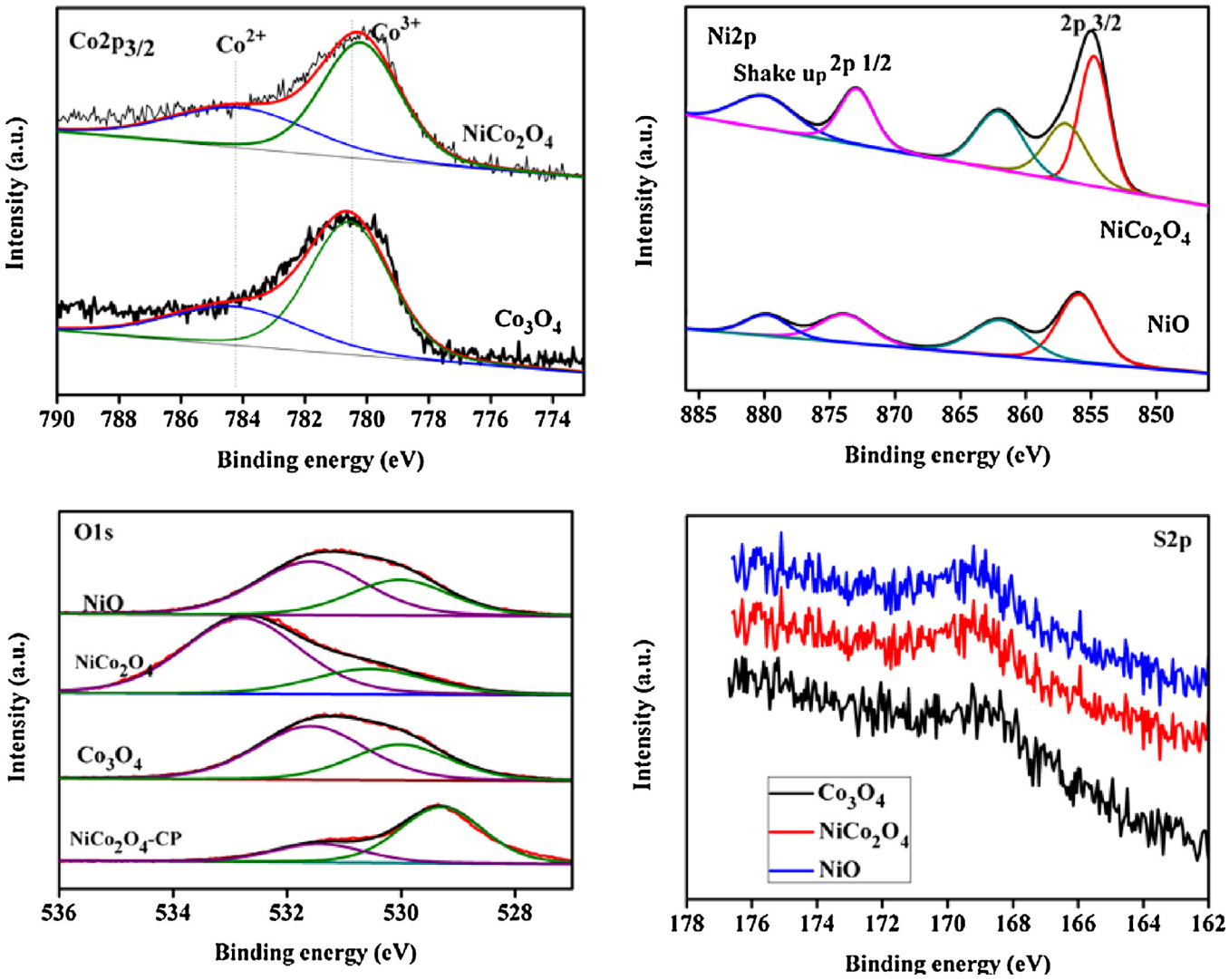

Fig. 10. XPS spectra of Co2p, Ni2p, O1s and S2p in fresh and sulfated catalysts.

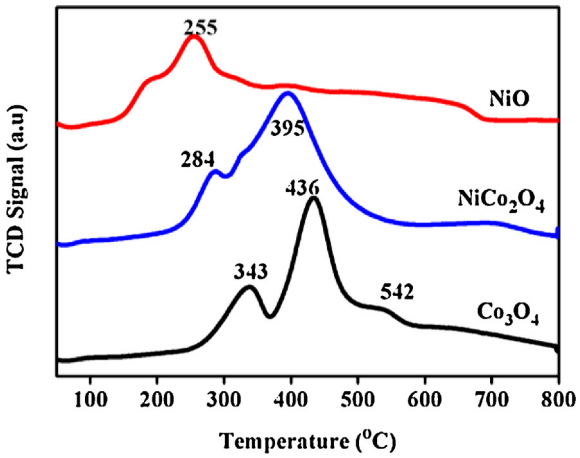

Fig. 11. The repeated H_2–TPR profiles of the sulfated Co_3O_4, NiO and $NiCo_2O_4$.

corresponding to two types of oxygen species. The low binding energy peak at 530.2 eV is related to lattice oxygen [20], while high one in Co_3O_4, NiO and $NiCo_2O_4$ occurs at 531.6–532.8 eV, corresponding to the surface-adsorbed oxygen species, which are derived from the adsorption of gaseous O_2 on oxygen vacancies [22,23]. The $O_{ads}/(O_{latt}+O_{ads})$ ratio in these catalysts follows the trend: Co_3O_4 < NiO < $NiCo_2O_4$ (Table 3). More oxygen vacancies in $NiCo_2O_4$ are probably related to its superior reduction ability at low temperature over NiO and Co_3O_4 [10c], which promotes the oxidation of NO to NO_2 at low temperature. Moreover, the $O_{ads}/(O_{latt}+O_{ads})$ ratio in $NiCo_2O_4$–CP (26.71%) are much lower than that of $NiCo_2O_4$ (75.06%), suggesting that the mesoporous structure may produce extra surface vacancies to activate oxygen, which could improve SCR performance at low temperature.

S2p XPS spectra of the sulfated Co_3O_4, NiO and $NiCo_2O_4$ are also shown in Fig. 10. The binding energy peak at 169.4 eV indicates the formation of sulfate species after exposure to SO_2 [18]. Surface sulfur contents in the sulfated Co_3O_4, NiO and $NiCo_2O_4$ are 0.24, 0.30 and 0.28% (Table 3), respectively. After Co_3O_4, NiO and $NiCo_2O_4$ are regenerated using H_2 at 550 °C for 30 min, sulfur contents are decreased to 0.11, 0.25 and 0.11%, respectively. Obviously, Co_3O_4 and $NiCo_2O_4$ show superior regenerability over NiO, which is consistent with their SCR activity in the regenerated catalysts (Fig. 6).

3.7. Repeated H_2–TPR

The repeated H_2–TPR experiments of the sulfated catalysts were performed to further investigate sulfur desorption performance, and the results are shown in Fig. 11. For Co_3O_4, the peak at 343 °C may be assigned to the reduction of Co_3O_4 to CoO, while the strong peak at 436 °C with a shoulder peak at 542 °C is related to the reduction of surface sulfates. A weak peak at 284 °C in $NiCo_2O_4$ may be assigned to the reduction of $NiCo_2O_4$ to $NiCoO_2$, and the broad peak at 395 °C corresponds to the reduction of surface sulfates. It should be mentioned that the sulfated NiO shows two peaks at 255 °C and 195 °C, which are related to the co-reduction of small amount of surface sulfates and NiO to Ni, respectively [21]. $NiCo_2O_4$ shows larger desorption peak areas of surface sulfates than Co_3O_4 and NiO, indicating that the sulfur desorption in $NiCo_2O_4$ is easier than that of the other two catalysts. As a result, $NiCo_2O_4$ possesses superior regeneration ability than Co_3O_4 and NiO in SCR.

4. Conclusions

A series of ordered mesoporous Co_3O_4, NiO and $NiCo_2O_4$ catalysts were prepared using mesoporous KIT-6 as a template. Compared with NiO and Co_3O_4, the bimetal $NiCo_2O_4$ exhibits better catalytic performance, wider temperature window over 150–400 °C, stronger resistance against SO_2 and H_2O as well as higher regeneration ability in H_2–SCR of NO_x. The superior SCR properties in $NiCo_2O_4$ are associated with the characteristic of ordered mesoporous structure, better low-temperature reducibility, more surface adsorption oxygen species as well as synergetic catalytic effect between Ni and Co ions. In summary, this study has demonstrated that highly ordered mesoporous bimetal oxides may serve as promising H_2–SCR catalysts at low temperature, which provides a possibility for the development of efficient low-temperature SCR catalysts.

Acknowledgement

This work was financially supported by Program (2011CBA00502, 2013CB933202), Major Project of Fujian Province (2013H0061).

Appendix A. Supplementary data

Supplementary data associated with this article can be found, in the online version, at http://dx.doi.org/10.1016/j.apcatb.2015.04.038.

References

[1] (a) D.Y. Yoon, J.H. Park, H.C. Kang, P.S. Kim, I.S. Nam, G.K. Yeo, J.K. Kil, M.S. Cha, Appl. Catal. B: Environ. 101 (2011) 275–282;
(b) X. Mou, B. Zhang, Y. Li, L. Yao, X. Wei, D. Su, W. Shen, Angew. Chem. Int. Ed. 51 (2012) 2989–2993.
[2] (a) K. Paredis, L.K. Ono, F. Behafarid, Z. Zhang, J.C. Yang, A.I. Frenkel, B.R. Cuenya, J. Am. Chem. Soc. 133 (2011) 13455–13464;
(b) C. Fang, D. Zhang, S. Cai, L. Zhang, L. Huang, H. Li, P. Maitarad, L. Shi, R. Gao, J. Zhang, Nanoscale 5 (2013) 9199–9207.
[3] (a) S. Fogel, D.E. Doronkin, P. Gabrielsson, S. Dahl, Appl. Catal. B: Environ. 125 (2012) 457–464;
(b) H. Chang, X. Chen, J. Li, L. Ma, C. Wang, C. Liu, J.W. Schwank, J. Hao, Environ. Sci. Technol. 47 (2013) 5294–5301;
(c) P.S. Kim, M.K. Kim, B.K. Cho, I.-S. Nam, S.H. Oh, J. Catal. 201 (2013) 65–76;
(d) A. Grossale, I. Nova, E. Tronconi, Catal. Today 136 (2008) 18–27.
[4] A. Väliheikki, K.C. Petallidou, C.M. Kalamaras, T. Kolli, M. Huuhtanen, T. Maunula, R.L. Keiski, A.M. Efstathiou, Appl. Catal. B: Environ. 156–157 (2014) 72–83.
[5] (a) F.J.P. Schott, P. Balle, J. Adler, S. Kureti, Appl. Catal. B: Environ. 87 (2009) 18–29;
(b) C.N. Costa, P.G. Savva, J.L.G. Fierro, A.M. Efstathiou, Appl. Catal. B: Environ. 75 (2007) 147–156;
(c) C.N. Cost, A.M. Efstathiou, Appl. Catal. B: Environ. 72 (2007) 240–252;
(d) R. Burch, M.D. Coleman, Appl. Catal. B: Environ. 23 (1999) 115–121.
[6] L. Li, P. Wu, Q. Yu, G. Wu, N. Guan, Appl. Catal. B: Environ. 94 (2010) 254–262.
[7] (a) G. Qi, R.T. Yang, F.C. Rinaldi, J. Catal. 237 (2006) 381–392;
(b) L. Li, F. Zhang, N. Guan, E. Schreier, M. Richter, Catal. Commun. 9 (2008) 1827–1832.
[8] F.M. Auxilia, S. Ishihara, S. Mandal, T. Tanabe, G. Saravanan, G.V. Ramesh, N. Umezawa, T. Hara, Y. Yu, S. Hishita, et. al, Adv. Mater. 26 (2014) 4481–4485.
[9] (a) J. Rosen, G.S. Hutchings, F. Jiao, J. Am. Chem. Soc. 135 (2013) 4516–4521;
(b) J. Li, S. Xiong, Y. Liu, Z. Ju, Y. Qian, ACS Appl. Mater. Interfaces 5 (2013) 981–988;
(c) J. Rosen, G.S. Hutchings, F. Jiao, J. Catal. 310 (2014) 2–9.
[10] (a) Y. Liu, L. Zou, J. Li, K. Guo, X. Dong, X. Li, X.H. Xue Zhang, H. Yang, Electrochim. Acta 129 (2014) 14–20;
(b) M. Khairy, S.A. El-Safty, M. Ismael, H. Kawarada, Appl. Catal. B: Environ. 127 (2012) 1–10;
(c) Y. Liu, H. Dai, J. Deng, S. Xie, H. Yang, W. Tan, W. Han, Y. Jiang, G. Guo, J. Catal. 309 (2014) 408–418;
(d) M. Chen, X. Zheng, J. Mol.r Catal. A 221 (2004) 77–80;
(e) S. Sun, Q. Gao, H. Wang, J. Zhu, H. Guo, Appl. Catal. B: Environ. 97 (2010) 284–297.
[11] (a) Y.J. Sa, K. Kwon, J.Y. Cheon, F. Kleitz, S.H. Joo, J. Mater. Chem. A 1 (2013) 9992–10001;
(b) F. Jiao, A.H. Hill, A. Harrison, A. Berko, A.V. Chadwick, P.G. Bruce, J. Am. Chem. Soc. 130 (2008) 5262–5266.
[12] Y. Liu, B. Liu, Q. Wang, C. Li, W. Hu, Y. Liu, P. Jing, W. Zhao, J. Zhang, J. Catal. 296 (2012) 65–76.
[13] Y. Gou, X. Liang, B. Chen, J. Alloys Compd. 574 (2013) 181–187.
[14] M. Richter, M. Langpape, S. Kolf, G. Grubert, R. Eckelt, J. Radnik, M. Schneider, M.-M. Pohl, R. Fricke, Appl. Catal. B: Environ. 36 (2002) 261–277.

[15] (a) X. Wang, Z. Chen, Y. Luo, L. Jiang, R. Wang, Sci. Rep. 3 (2013) 1559;
(b) X. Wang, Z. Chen, Y. Wang, R. Wang, ChemCatChem 6 (2014) 237–244;
(c) X. Wang, X. Qi, Z. Chen, L. Jiang, R. Wang, K. Wei, J. Phys. Chem. C 118 (2014) 13743–13751;
(d) X. Wang, L. Jiang, J. Wang, R. Wang, Appl. Catal. B: Environ. 165 (2015) 700–705.
[16] Y. Feng, L. Li, S. Niu, Y. Qu, Q. Zhang, Y. Li, W. Zhao, H. Li, J. Shi, Appl. Catal. B: Environ. 111–112 (2012) 461–466.
[17] H. Yen, Y. Seo, S. Kaliaguine, F. Kleitz, Angew. Chem. Int. Ed. 51 (2012) 12032–12035.
[18] S. Zuo, F. Liu, J. Tong, C. Qi, Appl. Catal. A Gen. 467 (2013) 1–6.
[19] L. Chen, Z. Si, X. Wu, D. Weng, ACS Appl. Mater. Interfaces 6 (2014) 8134–8145.
[20] S. Cai, D. Zhang, L. Shi, J. Xu, L. Zhang, L. Huang, H. Li, J. Zhang, Nanoscale 6 (2014) 7346–7353.
[21] J. Li, C. Wang, C. Huang, Y. Sun, W. Weng, H. Wan, Appl. Catal. A: Gen. 382 (2010) 99–105.
[22] C.Y. Ma, Z. Mu, J. Li, Y. Jin, J. Cheng, G. Lu, Z. Hao, S. Qiao, J. Am. Chem. Soc. 13 (2010) 2608–2613.
[23] G. Bai, H. Dai, J. Deng, Y. Liu, F. Wang, Z. Zhao, W. Qiu, C.T. Au, Appl. Catal. A: Gen. 450 (2013) 42–49.